integrity Research Journals

Applied Journal of Physical Science
Volume 6(4), pages 104-129, August 2025
Article Number: AB19CDD11
ISSN: 2756-6684
https://doi.org/10.31248/AJPS2025.120
https://integrityresjournals.org/journal/AJPS

Full Length Research

Energy transfer models of iron (II, III) oxide nanofluid in a chemically reacting porous medium

Samson Osinachi NWADIBIA*, Alalibo Thompson NGIANGIA and Hilary Patrick OBONG

Department of Physics, University of Port Harcourt, Port Harcourt, PMB 5323 Choba, Nigeria.

*Corresponding author. Email: osinachinwadibia777@gmail.com; Tel: +2348083058072.

Received 13th May 2025; Accepted 4th July 2025

ABSTRACT: The study of magnetohydrodynamics (MHD) nanofluid flow in a rectangular channel is presented using a numerical approach based on a mathematical model developed by combining the models of thermal conductivities and effective viscosity in addition to electroconductivity term and the approximation for the radiative heat flux vector for an optically thin medium at low density, was also deployed in the formalism. The resulting sets of partial differential equations were nondimensionalized based on the Buckingham-π using pertinent hydrodynamic variables, the coupled equations were solved using the Laplace Transform Technique for temperature, concentration and velocity. Graphical results presented show that the concentration, temperature are enhanced while the velocity diminishes as the nanoparticle volume fraction increases. The velocity increases alongside temperature as the parameter of the radiation term increases. The velocity field decreases along the axis and further decrease further as electroconductivity of the nanofluid increase. Furthermore, the velocity of the nanofluid decreases along the axis for all values of the Hartmann number. Implication of finding of the study is that the velocity of electrically conducting fluid is dampen as the conductivity and magnetic field intensity increase.

Keywords: Nanofluid, Iron (II) Oxide nanoparticle, water-based fluid, rectangular system, MHD.

INTRODUCTION

The evaluation of nanoparticle rotation and clustering effects caused by the high oscillating magnetic field on viscosity and thermal conductivity takes into account the influence of an oscillating magnetic force on the fundamental hydrodynamic equations. The effects of a high oscillating magnetic field and nanoparticle concentration on physical characteristics, mass, and heat transfer are thoroughly examined in this study. The graphical results show that a highly oscillating magnetic field rotates viscosity, thereby reducing overall viscosity and promoting a better nanoparticle dispersion or alignment. This, in turn, enhances thermal conductivity and thus, altered physical qualities contribute to improving the fluid flow and heat transfer rate (Hassan, 2018).

The analysis of the impacts of Fe3O4, SWCNT, and MWCNTs hybrid nanofluids with variable magnetic field on mass and heat transfer in a rectangular coordinate system was carried out in high-temperature environments involving high temperatures, thermal radiation is also taken into account. The hybrid nanofluid's governing equations are developed under specific, realistic physical conditions. These complex equations, which in most cases are nonlinear and analytically not solvable, are solved using numerical methods implemented in MATLAB through the parametric continuation method. They observed that as the volume proportion of nanomaterial increases, so does the thermal flow rate of the nanofluids. In their conclusion, they claimed that because the electrical current is nearly parallel to the magnetic field and the Lorentz force is low at the squeezing plate, the body force accelerates close to the boundary layer wall (Khan *et al*., 2022).

The study examines the temperature-dependent thermal conductivity of stable nanofluids, both aqueous and non-aqueous, stabilised with a surfactant monolayer and having an average particle size of 8 nm. Following their synthesis and characterisation, iron oxide (Fe_3O_4) nano-particles were functionalized with appropriate surfactants

and distributed across aqueous and nonaqueous-based fluids. Additionally, it was observed that the thermal conductivity of nanofluids increased with temperature, but nonaqueous nanofluids showed a reduction in this property. It's interesting to note that regardless of the type of base fluid, the ratio of thermal conductivity of both nanofluids to base fluids stays constant as the temperature rises. A result that shows the viscosity and thermal conductivity of nanofluids merely tracks those qualities of the base fluids, even if the viscosity of nanofluids drops with increasing temperature, while the viscosity ratio with regard to the base fluid stays constant. The average particle size does not change with temperature, according to an analysis of particle size and temperature. The results' implications show that the less significant contribution of microconvection to the improvement of thermal conductivity has been unequivocally confirmed (Shima *et al.*, 2010).

In a different study, titanium dioxide and Darcy–Forchheimer graphene oxide were evaluated for electrical conductivity entropy in a water hybrid nanofluid flow between two spinning disks. By applying a magnetic field, the flow conducts electricity and is saturated according to the Darcy-Forchheimer relation. Using the proper similarity transformations, the nonlinear governing equations are first transformed into ordinary differential equations. Then, using the Built-in-Shooting method, numerical solutions are determined. The results showed that the impacts of Bejan number and entropy generation rate against diffusion parameter are comparable. Additionally, the higher the Brinkman number, the higher the entropy formation rate (Khan *et al*., 2021).

In the investigation of the behaviour of Fe_2O_3 nanoparticles in a water-based nanofluid using the molecular dynamics (MD) method. The relationship between the viscosity of the Fe_2O_3-Water nanofluid and several parameters, such as the size, temperature, and content of nanoparticles, is investigated using the Green-Kubo technique, to guarantee the model's validity and dependability as well as the computational outcomes. The viscosity of the Fe_2O_3-water nanofluid is considerably higher than that of the water-based fluid (>57%), according to the results. Additionally, it is shown that the viscosity of the nanofluid reduces with temperature and the size of nanoparticles with local sensitivity and increases with the particle volume fraction. Additionally, they found that the presence of nanoparticles produced a structured water layer close to the nanoparticle surface and that the iron-oxygen of water pair interactions were dominated by interactions between water molecules and iron oxide nanoparticles (Sadeghi *et al.,* 2023).

Fe_3O_4 nanoparticles added to Al_2O_3 in water nanofluid slightly reduce the motion of the flow at all points from the wall to the free stream, according to the results of a three-dimensional flow of water conveying alumina nanoparticles and water conveying alumina/iron (III) oxide nanoparticles within the thin boundary layer formed on a bidirectional linearly stretchable surface. Nonetheless, it was also noted that the temperature distribution throughout the flow had improved (Koriko *et al*., 2020).

Fe_3O_4-Al_2O_3-TiO_2 ternary hybrid nanoparticles were used in a novel way to investigate the enhancement technique and analyse the thermal behaviour of a non-Newtonian Casson fluid. Ternary hybrid nanoparticles have enhanced the fluid's overall thermal conductivity, which has led to a significant increase in the temperature distribution, according to a numerical analysis of the study's governing equation using the Galerkin finite element methodology (Kaneez *et al*., 2023).

The effects of magnetic field-dependent viscosity on unsteady water-based Fe_3O_4 magnetic fluid flow over a rotating and vertically moving disk are described by physical models. The research indicates that the fluctuations in viscosity caused by the alternating magnetic field are contingent upon both the magnetic field's strength and frequency changes. Additionally, according to Bhandari *et al.* (2023), an oscillating magnetic field causes more friction on the disk than a fixed magnetic field.

Suspension of magnetite Fe_3O_4 in water-based nanofluids was adopted as the working fluid in the experimental evaluation of the effect of magnetic field strength on heat transfer enhancement of different turbulent flows of Fe_3O_4 in water nanofluids and with different concentrations in a pipe heated with constant heat flux intensity. The investigation's findings showed that, for both water and nanofluids, the Nusselt number (Nu) rises when Re increases, whether a magnetic field is present or not. Higher values than water were also obtained. Additionally, the pressure loss rises as the Reynolds number and magnetic field strength do. Compared to the thermal motion of magnetic nanoparticles, it can be inferred that the magnetic field significantly affects the Fe3O4/water nanofluid's thermal transfer capability. Lastly, it is discovered that both with and without a strong magnetic field, the performance factor is more than unity (Ebaid *et al.*, 2022).

The experimental assessment of glycerol and α-Fe_2O_3 nanoparticle nanofluids' rheological characteristics. According to the findings, the viscosity of α-Fe_2O_3-glycerol nanofluids rises as the particle volume fraction increases and falls as the temperature rises. The evaluation's findings unequivocally demonstrated that the α-Fe_2O_3-glycerol nanofluids are non-Newtonian shear-thinning and that temperature has a significant impact on their shear viscosity (Abareshi *et al*., 2011).

Since some lubrication systems are reproductions of Taylor Couette flow, it is crucial to experimentally assess the influence of magnetic fields on Fe_3O_4 in water-based nanofluids undergoing this type of flow. For nanofluid in the presence of a magnetic field, it was found that the critical frequency for different transitions decreases with the volume fraction of nanoparticles; however, for nanofluid in the absence of a magnetic field, the pattern was inconsistent (Muritala *et al*., 2022).

The assessment of the importance of Fe_2O_3 nanoparticles' improvement of heat transfer in the flow across a revolving disk. It has been noted that when the volumetric concentration of nanoparticles increases, the radial velocity decreases while the tangential motion of flow increases. Additionally, the nanofluid's free motion around the revolving disk is resisted by the high magnetic force 0≤m1≤6 (Farooq *et al*., 2023).

For oil recovery applications at the laboratory scale, a new improved antenna is utilised in conjunction with iron oxide (Fe_2O_3) and zinc oxide (ZnO) nanofluids. The diameters of the iron oxide (Fe_2O_3) nanoparticles ranged from 30.27 to 37.60 nm (Yahya *et al.* 2014). In comparison to the case without magnetic feeders, the experimental analysis found that the curve antenna with magnetic feeders produced a 78% increase in the magnetic field signal intensity. When compared to the case without magnetic feeders, the electric field signal strength increased by 473% with the curve antenna equipped with magnetic feeders.

MATERIALS AND METHODS

Mathematical formulation of the problem

We considered a flow of an electrically conducting water-based Iron (II, III) oxide nanofluid in a rectangular channel through a porous medium, acting upon the fluid is a homogenous magnetic field. The governing equations representing the parameters under the flow condition of the study are the equations of Continuity, Momentum, Energy and Concentration in Cartesian coordinates. In a situation where the water-based Iron (II, III) oxide nanofluid is considered incompressible, and is subjected to a steady state flow condition transformed into:

$$\frac{\partial}{\partial x}v_x = 0 \quad (1)$$

$$v_x\frac{\partial v_x}{\partial x} = \frac{\mu_{nf}}{\rho_{nf}}\left(\frac{\partial}{\partial x}\left(\frac{\partial v_x}{\partial x}\right)\right) + \frac{g\beta^C(C-C^*)}{\rho_{nf}} + \frac{g\beta^T(T-T^*)}{\rho_{nf}} - \frac{\sigma {B_0}^2 v_x}{\rho_{nf}} \quad (2)$$

$$v_x\frac{\partial T}{\partial x} = \frac{K_{nf}}{(\rho\hat{C_p})_{nf}}\left(\frac{\partial}{\partial x}\left(\frac{\partial T}{\partial x}\right)\right) - \frac{1}{(\rho\hat{C_p})_{nf}}\frac{\partial q_z}{\partial y} \quad (3)$$

$$\frac{\partial C}{\partial t} + v_x\frac{\partial C}{\partial x} = \frac{D}{(\rho\hat{C_p})_{nf}}\left(\frac{\partial}{\partial x}\left(\frac{\partial C}{\partial x}\right)\right) + \frac{K_0^2 C}{(\rho\hat{C_p})_{nf}} \quad (4)$$

Where B_o is uniform magnetic field strength, σ is electrioconductivity, ρ_{nf} is the density of nanofluid, μ_{nf} is the viscosity of nanofluid, β^c is the concentration expansivity, β^T is the thermal expansivity α, K_{nf} is thermal conductivity of nanofluid, v_x is velocity fluid component, T is temperature of nanofluid, T^* is the temparure at the wall, C_p is specific heat at constant pressure, t is the time, C is the concentration of nanofluid, C^* is the concentration at the wall, g is acceleration due to gravity, q_x is the radiation energy flux term, K_o is chemical reaction term, D is chemical molecular diffusivity, x is axis of the rectangular system under consideration. Invoking the electro-conductivity model of fluid assumed by Boričić *et al*. (2005) in their study of MHD universal equation with variable electro-conductivity on a heated moving plate, where they presented an electro-conductivity term given by:

$$\sigma_o = \sigma_\infty\left(1 - \frac{u}{U}\right) \quad (5)$$

where u is the average longitudinal velocity, U is the plate's velocity, σ_∞ is the electroconductivity at a point from the origin, σ_o is the electroconductivity at the origin.

Following the work of Ngiangia and Jim-George (2019), the approximation of the electroconductivity term proposed in equation 5 is transformed into

$$v_x\frac{\partial v_x}{\partial x} = \frac{\mu_{nf}}{\rho_{nf}}\left(\frac{\partial}{\partial x}\left(\frac{\partial v_x}{\partial x}\right)\right) + \frac{g\beta^C(C-C^*)}{\rho_{nf}} + \frac{g\beta^T(T-T^*)}{\rho_{nf}} - \frac{\sigma {B_0}^2 v_x}{\rho_{nf}} - \frac{\sigma_\infty u'}{U} \quad (6)$$

Considering the viscous and thermal conductivity models is a combined model of viscosity proposed by Vand (1948) and De Bruijn (1948), and a combined model of thermal conductivity proposed by Kumar *et al.* (2004) and Bhattacharya *et al.* (2004) are respectively presented

$$\mu_{eff} = \{1 + 25\phi_p + 3125\phi_p^2 + \ldots\}\mu_b + (1 + 2.5\phi_p + 4.698\phi_p^2 + \ldots)\mu_b \quad (7)$$

$$\frac{\partial C}{\partial t} + v_x\frac{\partial C}{\partial x} = \frac{D}{(\rho\hat{C_p})_{nf}}\left(\frac{\partial}{\partial x}\left(\frac{\partial C}{\partial x}\right)\right) - \frac{K_0^2 C}{(\rho\hat{C_p})_{nf}} \quad (8)$$

Where ϕ_p is the nanoparticle volume fraction, μ_b is the dynamic viscosity of the base fluid, K_B is the Stefan Boltzmann's constant, c is a constant, v is the dynamic velocity of the base fluid, T is the temperature, r_b is the thickness radius of the base fluid, r_p is the thickness radius of the nanoparticle, d_p is the diameter of the nanoparticle, k_b is the thermal conductivity of the base fluid, k_p is the thermal conductivity of nanoparticle, π is a constant that is taken to be 3.14.

The radiative heat flux vector q_z of the energy equation (6) is related to the temperature by the expression.

$$\frac{\partial^2 q_z}{\partial y^2} - 3\sigma_c^2 - 16\sigma_c T_\infty^3\frac{\partial T}{\partial y} = 0 \quad (9)$$

And according to the model proposed by Cogley *et al.* (1968) for an optically thin medium at a relatively low density, the expression for the radiative heat flux vector reduces to:

$$\frac{\partial q_z}{\partial y} = 4\alpha^2(T_o - T_w) \quad (10)$$

Where $\alpha^2 = \int_0^\infty\left(\delta_k\frac{\partial\omega}{\partial T}\right)dk^*$ referred to as the frequency

dependent absorption coefficient, δ_k is the mean absorption coefficient, σ is the Stefan-Boltzmann's constant, ω is the Planck's function, T_o is the temperature at the center, and T_w is the temperature at the wall. Transforming the energy equation of equation (6) based on the consideration of the radiative flux term presented in equation (10), the energy equation becomes.

$$v_x \frac{\partial T}{\partial x} = \frac{K_{nf}}{(\rho \hat{C_p})_{nf}} \left(\frac{\partial}{\partial x} \left(\frac{\partial T}{\partial x} \right) \right) - \frac{v_x}{(\rho \hat{C_p})_{nf}} 4\alpha^2 (T_o - T_w) \quad 11$$

Based on the study of Khalid *et al.* (2015) on convective flow of nanofluid with wall at ramped temperature, and Tiwari and Das (2007) on the augmentation of heat transfer of nanofluid on two sided lid driven differential heat cavity, the density of the nanofluid (ρ_{nf}), thermal expansion due to the temperature of the nanofluid (βnf), thermal expansion due to concentration of nanofluid (β^*_{nf}), and specific heat at constant pressure of the nanofluid $(Cp)_{nf}$ are respectively defined as:

$$\frac{\rho_{nf}}{\rho_f} = (1-\phi) + \phi \frac{\rho_s}{\rho_f} \quad 12$$

$$\frac{\beta_{nf}}{\beta_s} = (1-\phi) + \phi \frac{\beta_s}{\beta_f} \quad 13$$

$$\frac{\beta^*_{nf}}{\beta^*_s} = (1-\phi) + \phi \frac{\beta^*_s}{\beta^*_f} \quad 14$$

$$\frac{(C_p)_{nf}}{(C_p)_f} = (1-\phi) + \phi \frac{(C_p)_s}{(C_p)_f} \quad 15$$

The constant values of some of the thermophysical properties of the materials are presented in Table 1

Dimensional analysis

In order to tackle the set of coupled partial differential equations developed based on the mathematical formalism of the problem, the Buckingham-π is used to nondimensionalize the governing coupled equation by using the following hydrodynamic dimensionless variables representing specific boundary layer conditions of the flow;

$$u = \frac{v_x t^1}{x^1}, r = \frac{x^1}{d}, t = \frac{t^1}{u^1 t^1}, Re^{-1} = \frac{\mu_{nf}\rho_f}{\rho_{nf}\mu_f}, Pr^{-1} = \frac{k_{nf}(\rho C_p)_f}{k_f(\rho Cp)_{nf}}, Sc^{-1} = \frac{D(\rho C_p)_f}{k_f(\rho C_p)_{nf}},$$

$$k_0 = \frac{k_x^2(\rho C_p)_f}{(\rho C_p)_{nf} x^{*2}}, Gr_\theta = \frac{g\beta_{nf}(T-T_0)\mu_{nf}}{v_0 u^2 \beta_f}, Gr_c = \frac{g\beta^*_{nf}(C-C_0)\mu_{nf}}{v_0 u^2 \beta^*_f}, \theta = \frac{T-T_0}{T_0}, C = \frac{C-C_0}{C_0},$$

$$W = \frac{4\delta d^2}{\upsilon}, M = \frac{\sigma_0 B^2 v_x}{\rho_{nf}}, \quad \epsilon_o = \frac{\sigma_\infty \mu_b dt}{U}$$

Substituting the dimensionless variables into the governing equations transforms them into

$$\frac{\partial u}{\partial x} = 0 \quad 16$$

$$u\frac{\partial u}{\partial x} = \frac{A_1}{Re}\left(\frac{\partial^2 u}{\partial x^2}\right) + A_2 Gr_m C + A_3 Gr_t \theta - A_4(M+\epsilon_o)u \quad 17$$

$$u\frac{\partial \theta}{\partial x} = \frac{A_5}{Pr}\left(\frac{\partial^2 \theta}{\partial x^2}\right) + A_6 W\theta \quad 18$$

$$u\frac{\partial C}{\partial x} = \frac{A_6}{Sc}\left(\frac{\partial^2 C}{\partial x^2}\right) + A_6 k_o C \quad 19$$

Where *Re* is the Reynolds number, *Pr* is the Prandtl number, *Sc* is the Schmidt number, $G_{r_\theta}\theta$ is the thermal Grashof number, G_{r_c} is Grashof's number due to concentration, W is a dimensionless radiation term, θ is dimensionless temperature, *u* is dimensionless velocity, *C* is dimensionless concentration, M is the magnetic Hartmann number, k_0 is dimensionless chemical reaction term and *r* is the dimensionless radius of nanoparticles, ϵ_o is the electrical conductivity term.

From equation 20 to equation 23, the ratio of the effective dynamic viscosity terms and the effective thermal conductivity can be expressed as:

$$A_1 = \frac{1+25\phi_p+3125\phi_p^2+1+2.5\phi_p+4.698\phi_p^2}{(1-\phi)+\phi\frac{\rho_s}{\rho_f}}, \quad A_2 = (1-\phi)+\phi\frac{\beta_s}{\beta_f},$$

$$A_3 = \frac{\beta^1_{nf}}{\beta^1_s} = (1-\phi)+\phi\frac{\beta^1_s}{\beta^1_f}, \quad A_4 = \frac{1}{\left((1-\phi)+\phi\frac{\rho_s}{\rho_f}\right)}, \quad A_5 = \frac{\left(K_b + C\frac{2K_B T}{(\pi v d_p^2)K_b(1-\phi)r_p}\frac{\phi r_b}{K_b} + \phi K_p + (1-\phi)K_b\right)}{\left((1-\phi)+\phi\frac{(C_p)_s}{(C_p)_f}\right)}, A_6 = \frac{1}{\left((1-\phi)+\phi\frac{(C_p)_s}{(C_p)_f}\right)}$$

Solution Technique

Integrating equation 24 shows that:

$$u = c \quad 20$$

And when we assume *c = 1*, while considering the solution in other set of equations, our governing equations are simplified into;

$$\frac{A_1}{Re}\left(\frac{\partial^2 u}{\partial x^2}\right) - \frac{\partial u}{\partial x} + A_2 Gr_m C + A_3 Gr_t \theta - A_4(M+\epsilon_o)u = 0 \quad 21$$

$$\frac{A_5}{Pr}\left(\frac{\partial^2 \theta}{\partial x^2}\right) - \frac{\partial \theta}{\partial x} + A_6 W\theta = 0 \quad 22$$

$$\frac{A_6}{Sc}\left(\frac{\partial^2 C}{\partial x^2}\right) - \frac{\partial C}{\partial x} + A_6 k_o C = 0 \quad 23$$

Table 1. Numerical values of thermophysical properties of our materials.

Properties	Materials	
	Iron (II, III) oxide (Fe_3O_4)	Water (H_2O)
Density ρ (kgm^{-1})	5180	997.1
Thermal conductivity k (kgm^{-1})	9.7	0.613
Heat capacity C_p $(Wm^{-1}k^{-1})$	670	4179
Thermal expansivity k (kgm^{-1})	0.5×10^{-5}	21×10^{-5}

Table 2. Selected values of dimensionless hydrodynamic parameters.

Parameters	Selected values			
Reynolds number (*Re*)	1500	2500	3500	4500
Prandtl number (*Pr*)	2.7	4.7	6.7	8.7
Schmidt number (*Sc*)	1.5	3.5	5.5	7.5
Thermal Grashofs number (*Grθ*)	3	6	9	12
Modified Grashof number (*GrC*)	3.5	5.5	7.5	9.5
Radiation term (*W*)	1	3	5	7
Magnetic Number (*M*)	7	14	21	28
Chemical reaction term (*k*)	2	5	8	11
Electro-conductivity term (ϵ_o)	10	20	30	40
Nanoparticle volume fraction	0.03	0.06	0.09	0.012

Table 3. Numerical values of coefficients of the hydrodynamic parameters of the dimensionless governing equation when ϕ = 0.03.

Coefficient	Numerical value
A_1	1.916
A_2	0.973
A_3	0.971
A_4	1.126
A_5	0.777
A_6	0.995

Solving 25, 26, and 27 using Laplace Transform Technique, to obtain the concentration field, temperature field and velocity field.

$$\bar{C}(s) = \frac{\frac{A_6}{Sc} - 1}{\left(\frac{A_6}{Sc}s^2 - s - A_6 k_o\right)} \quad 24$$

$$\bar{\theta}(s) = \frac{\frac{A_5}{Pr} + 1}{\left(\frac{A_5}{Pr}s^2 - s + A_6 W\right)} \quad 25$$

$$\bar{U}(s) = \frac{\left(\frac{A_1}{Re} - 1\right) - A_2 Gr_m \left(\frac{\frac{A_6}{Sc} - 1}{\left(\frac{A_6}{Sc}s^2 - s - A_6 k_o\right)}\right) - A_3 Gr_t \left(\frac{\frac{A_5}{Pr} + 1}{\left(\frac{A_5}{Pr}s^2 - s + A_6 W\right)}\right)}{\left(\frac{A_1}{Re}s^2 - s - A_4 M - A_4 \sigma_o\right)} \quad 26$$

RESULTS AND DISCUSSION

Results of the various nanoparticle profiles are presented in Figures 1 to 17 according to the numerical values presented in Table 1, Table 2 and the computed values of Tables 3.

Temperature field

The results in Figure 2 show the temperature profile of the nanofluid as the value of the nanoparticles volume fraction increases. The pattern of results obtained shows that as the nanoparticles volume fraction increases, the temperature of the nanofluid samples is enhanced but diminishes along the axis. The physical implication of the result here is that in a situation where the concentration of Iron (II, III) oxide nanoparticles increases in the base fluid, the temperature decreases along the axis and increases slightly as the concentration of the Iron (II, III) oxide nanoparticles increases. The result presented for the combined thermal conductivity model is at a higher temperature value, as the volume fraction of Iron (II, III) oxide nanoparticle increases. The results here are in good agreement with the report of Ojjela (2022), Singh *et al*. (2016), Dogonchi *et al.* (2017) and Hady *et al.* (2012).

The result profiles presented in Figure 3 display a pattern of trends that show how temperature decreases as displacement along the *x*-axis increases. Also observed from the result profile is the decrease in the temperature field as the Prandtl number increases. Physically, the

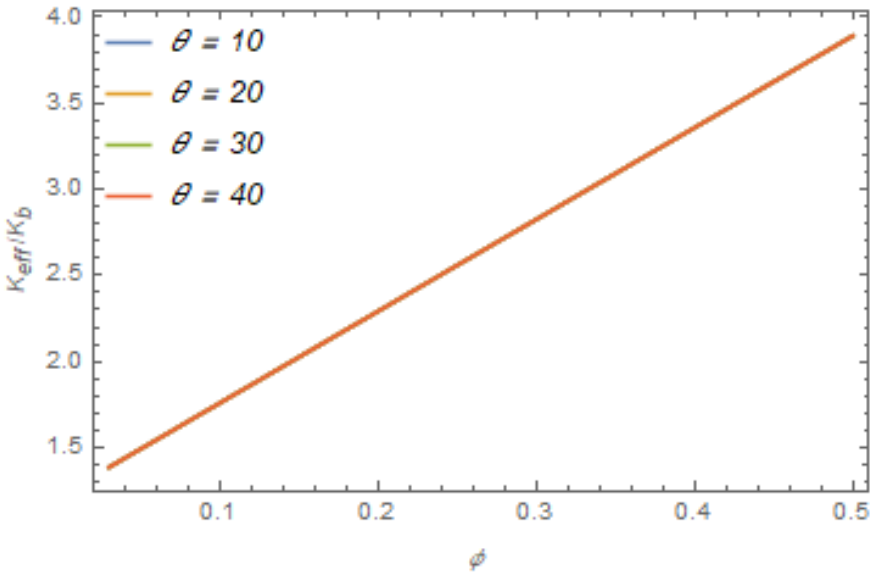

Figure 1. Profile of effective thermal conductivity ratio against nanoparticle volume fraction for varying temperature.

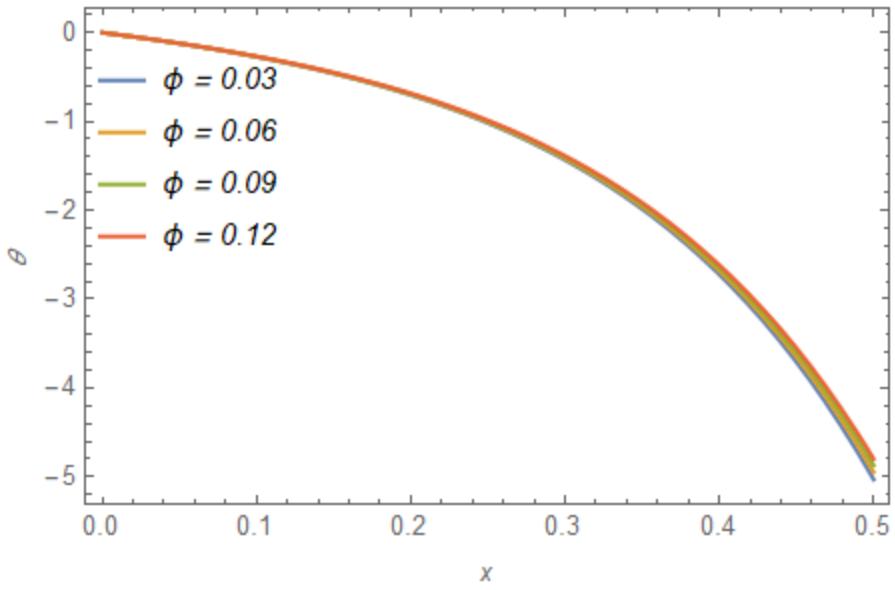

Figure 2. Profile of temperature for increasing value of nanoparticles volume fraction.

results obtained imply that in a flow situation where momentum transfer dominates the thermal transfer motivated in the combined model, the temperature of Iron (II, III) oxide water-based nanofluid increases as a result of an increase in the dominance. Our result agrees excellently with the results of Sarkar *et al*. (2024), Hsiao (2017), Hayat *et al*. (2021), and Jalili *et al*. (2023). The result disagrees with the result presented by Kataria and Mittal (2017).

In Figure 4, the profile of the result obtained shows that temperature decreases as displacement along the x-axis increases, and drops further as the radiation term increases. Physically, the results obtained imply that the temperature of Iron (II, III) oxide water-based nanofluid diminishes as a result of increased thermal layer. The result in this study agrees excellently with Rout and Mishra (2018) but disagrees with the result reported by Farooq *et al*. (2024), Dogonchi *et al*. (2017), Hady *et al.* (2012), and Gupta *et al*. (2024), but a contrary conclusion was presented by Aminuddin *et al.* (2023).

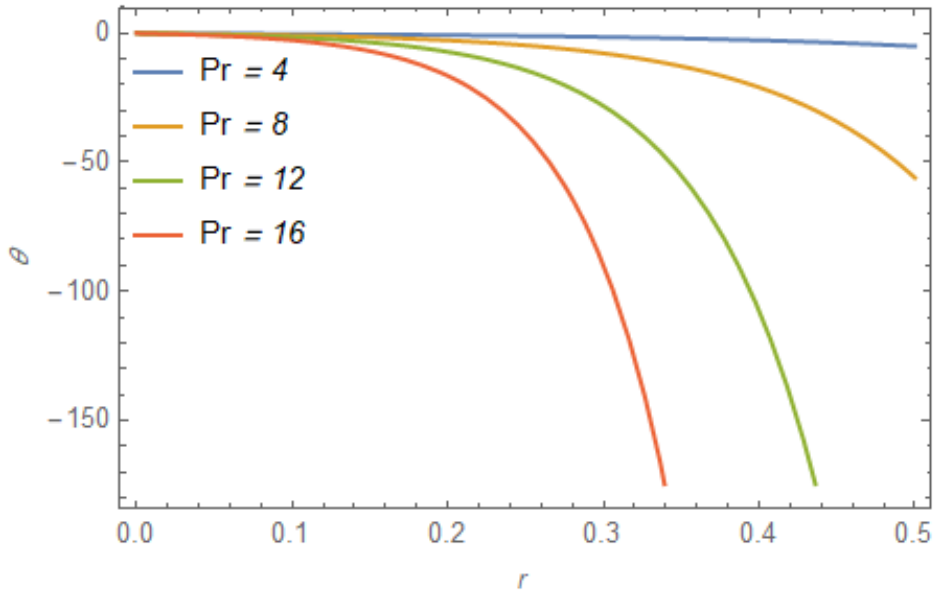

Figure 3. Temperature profile against axial distance for increasing Prandtl number.

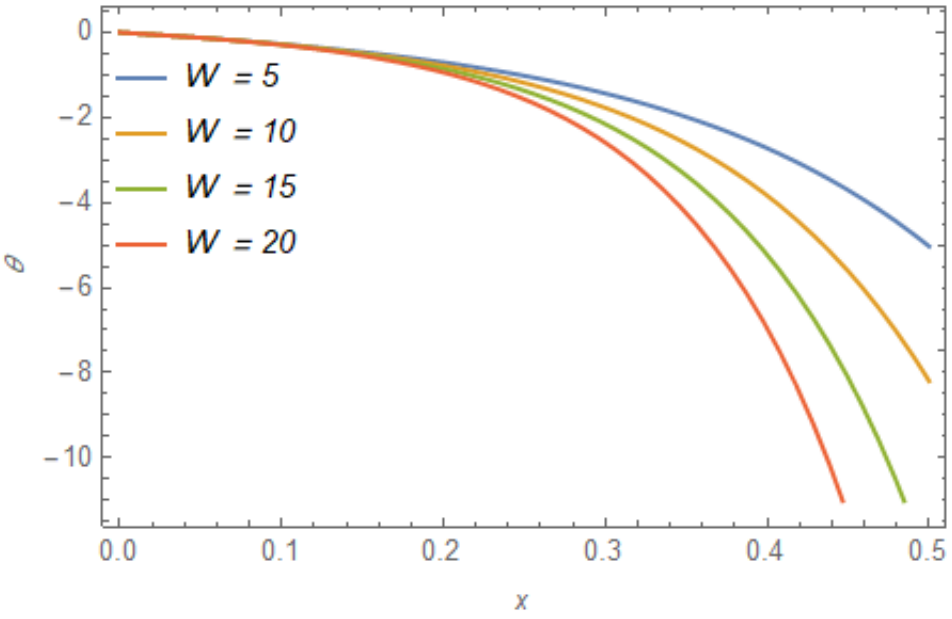

Figure 4. Temperature profile against axial distance for increasing radiation term of Iron (II, III) oxide nanofluid.

Concentration field

In Figure 5, the result of the concentration profile for varying values of the chemical reaction term shows that concentration decreases as displacement along the x-axis increases. Results also reveal that a decrease in concentration is caused by the increase in the chemical reaction term. The concentration of Iron (II, III) oxide water based nanofluid increases as a result on increase in the dominance. The result agrees excellently with the result obtained by Krishna *et al.* (2021), Gupta *et al.* (2024).

In Figure 6, the result of the concentration profile for varying values of nanoparticle volume fraction shows that concentration decreases as displacement along the x-axis increases. Also observed from the result profile is the increase in concentration as the Iron (II, III) oxide

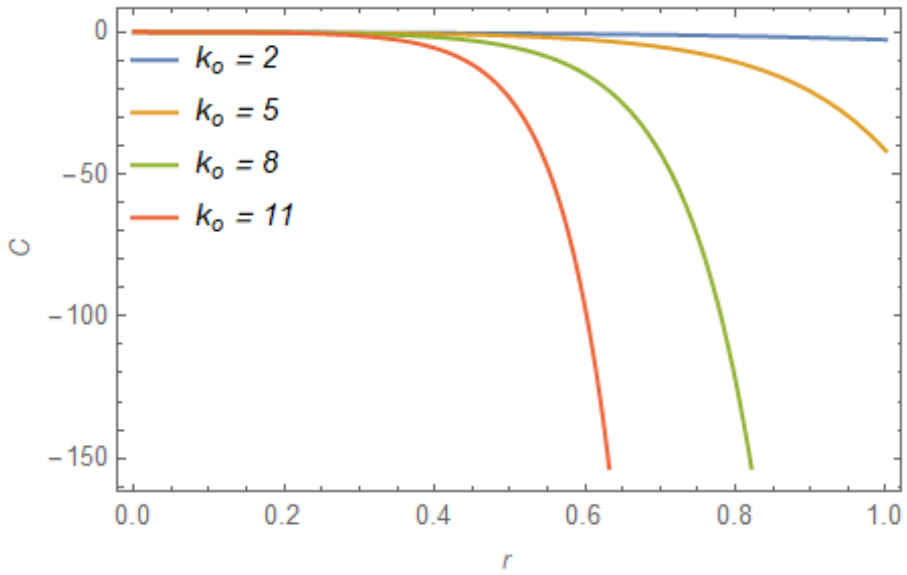

Figure 5. Concentration profile against axial distance for increasing chemical reaction term of Iron (II, III) oxide nanofluid.

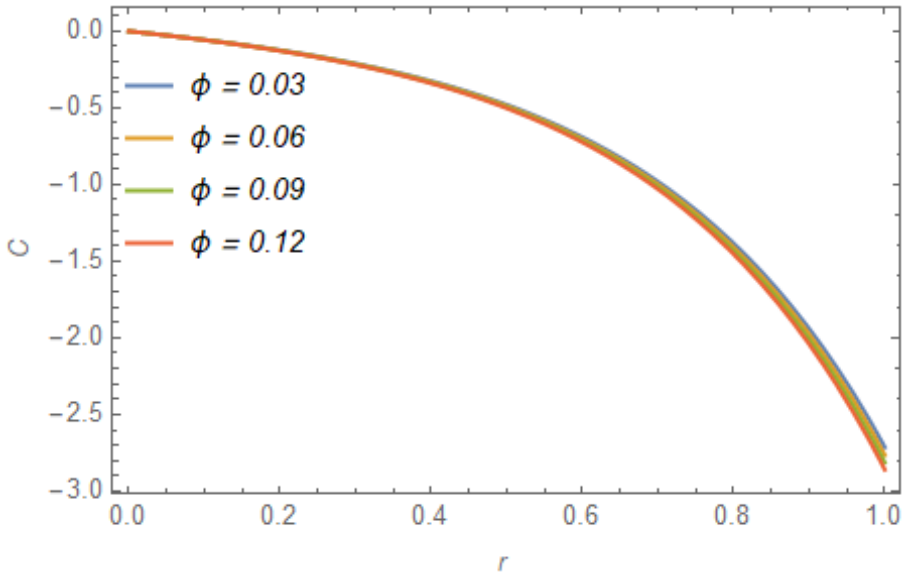

Figure 6. Concentration profile against axial distance for increasing nanoparticle volume fraction of Iron (II, III) oxide nanofluid.

nanoparticle volume fraction increases.

In Figure 7, the result of the concentration profile for varying values of Schmidt number shows that concentration decreases as displacement along the x-axis increases. And, further shows that the decrease in concentration as the Schmidt number increases. The result agrees excellently with Hsiao (2017), Madhukesh *et al.* (2023), Batool *et al.* (2022), Hamid *et al.* (2019), Hayat *et al.* (2021), Jalili *et al.* (2023), Krishna *et al.* (2021), Kataria and Mittal (2017), and Gupta *et al.* (2024).

Velocity field

In Figure 8, the graphical profile of velocity along the axis is shown for increasing values of the thermal Grashof number. The pattern of results in the profile reveals how the velocity of the water-based Iron (II, III) oxide decreases with successive increases in the values of the thermal Grashof number. The pattern of results presented also shows that the velocity of Iron (II, III) oxide nanofluid decreases along the axis for all values of the thermal

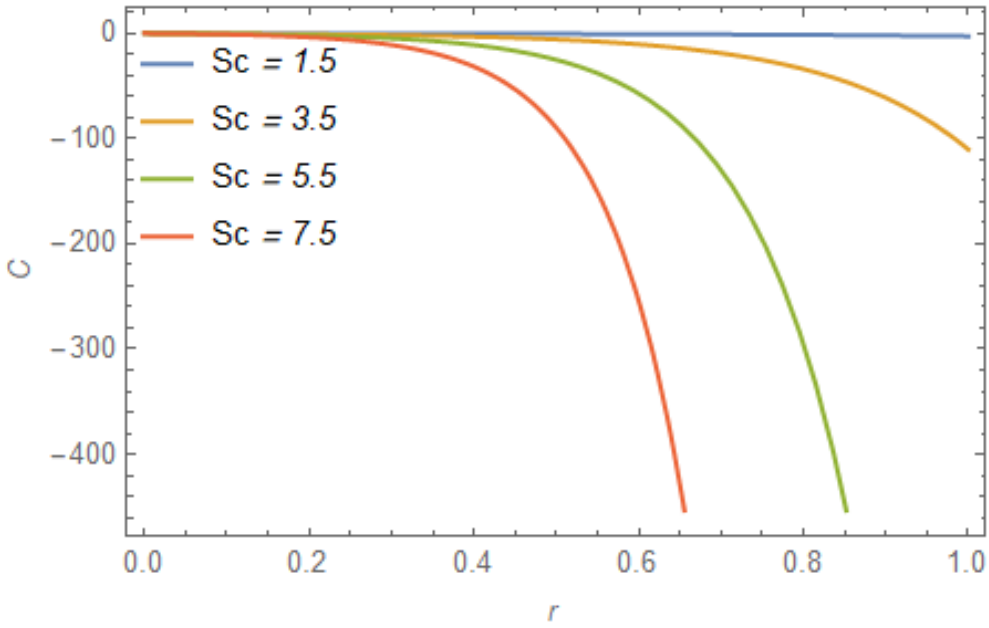

Figure 7. Concentration profile against axial distance for increasing Schmidt number of Iron (II, III) oxide nanofluid.

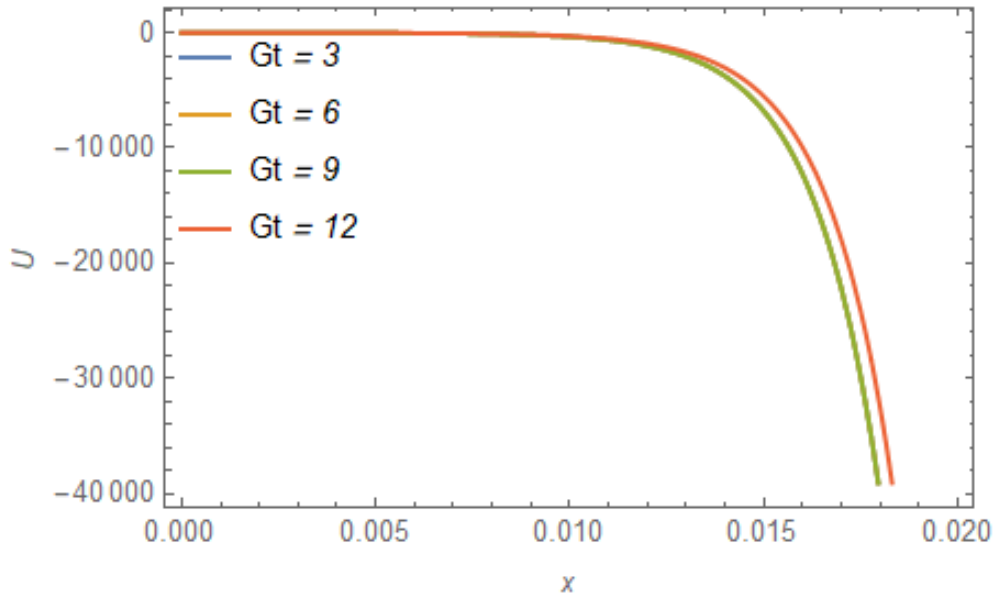

Figure 8. Velocity profile against axial distance for increasing thermal Grashof number.

Grashof number. The result agrees with the report presented by Hayat *et al.* (2021). A contrary report was given by Rammoorthi and Mohanavel (2023), Krishna *et al.* (2021), and Kataria and Mittal (2017).

In Figure 9, the result pattern obtained in the profile reveals how the velocity of the water-based Iron (II, III) oxide decreases with a sequential increase in the values of the modified Grashof number. The pattern of results presented also shows that the velocity of Iron (II, III) oxide nanofluid decreases along the axis for all values of the modified Grashof number. The result of this study disagrees with the results presented by Krishna *et al.* (2021), Kataria and Mittal (2017) and Kataria and Mittal (2015).

In Figure 10, the trendlines show how the water-based Iron (II, III) oxide's velocity is unresponsive to the

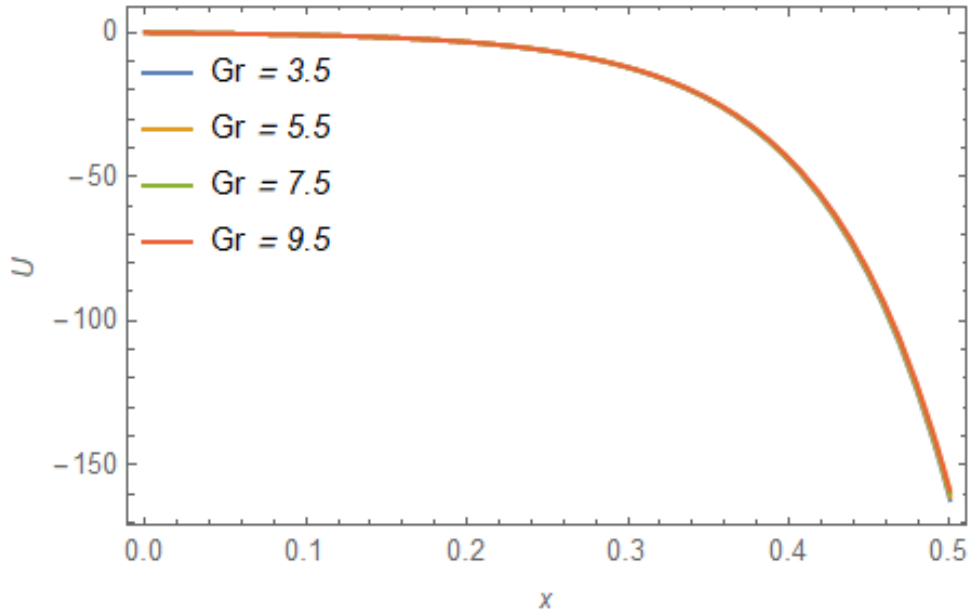

Figure 9. Velocity profile against axial distance for increasing modified Grashof number.

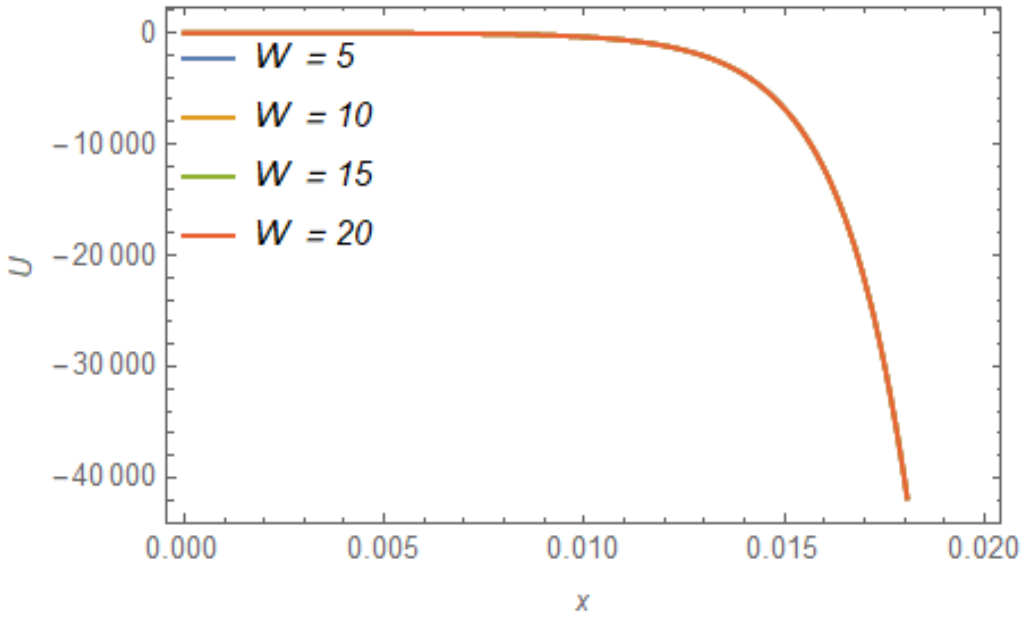

Figure 10. Velocity profile against axial distance for increasing radiation term.

subsequent rise in radiation parameter values. For all values of the radiation parameter, the pattern of results also demonstrates that the velocity of the Iron (II, III) oxide nanofluid decreases down the axis. The results presented by Kataria and Mittal (2015) reveal that there is an elevation in the velocity of the nanofluid as the parameter increases.

In Figure 11, the pattern of results in the profile of velocity along the radial axis for increasing values of the chemical reaction term shows that the velocity of Iron (II, III) oxide nanofluid decreases along the radial axis for all values of the chemical reaction term. Result presented also reveal that changing chemical reaction term does not affect the velocity.

In Figure 12, the profile of velocity along the axis is shown for increasing values of the Hartmann number. The pattern of results in the profile shows how the velocity of the water-based Iron (II, III) oxide increases for successive

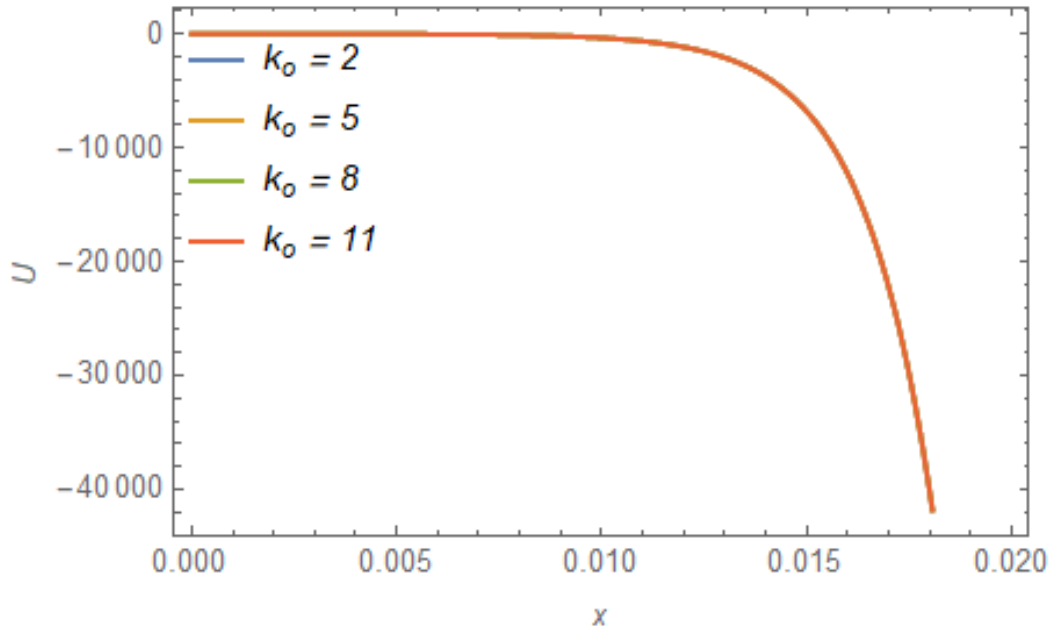

Figure 11. Velocity profile against axial distance for increasing chemical reaction term.

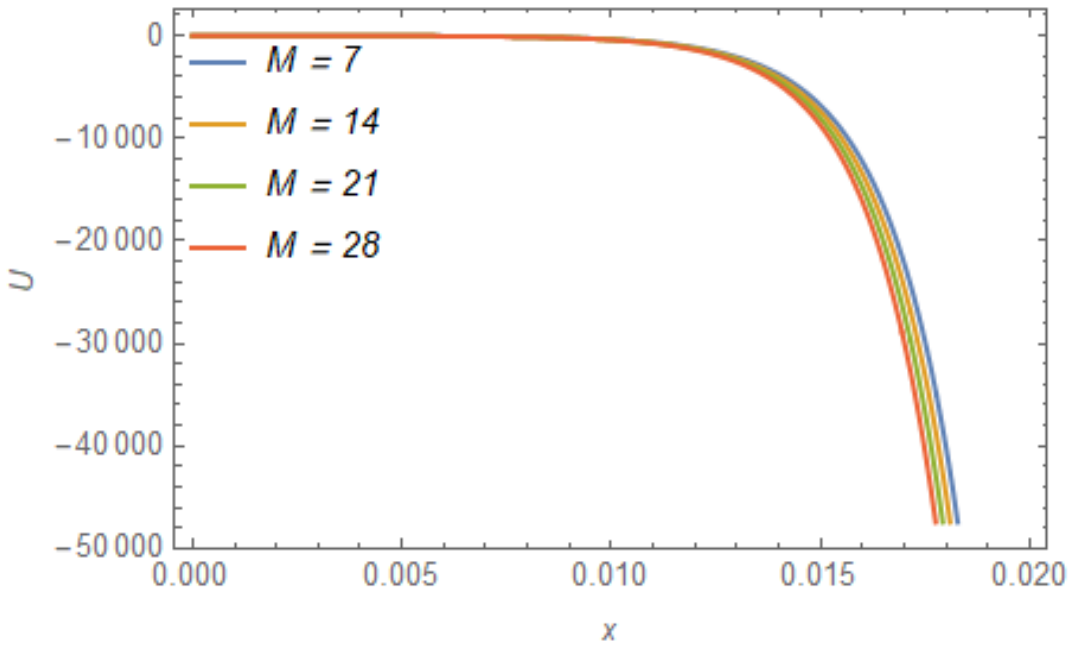

Figure 12. Velocity profile against axial distance for increasing magnetic hartmantn number.

increases in values of the Hartmann number. The pattern of results presented also shows that the velocity of Iron (II, III) oxide nanofluid decreases along the axis for all values of the Hartmann number. A contrary result was presented by Aminuddin *et al*. (2023). But agrees excellently with the results of Kataria and Mittal (2015), Kataria and Mittal (2017), Rammoorthi and Mohanavel (2023), Jalili *et al.* (2023), and Hsiao (2017).

In Figure 13, the graphical profile of velocity along the axis is shown for increasing values of the Prandtl number. The pattern of results in the profile reveals how the velocity of the water-based Iron (II, III) oxide also overlaps for a continuous increase in values of the Prandtl number. The pattern of results presented also shows that the velocity of

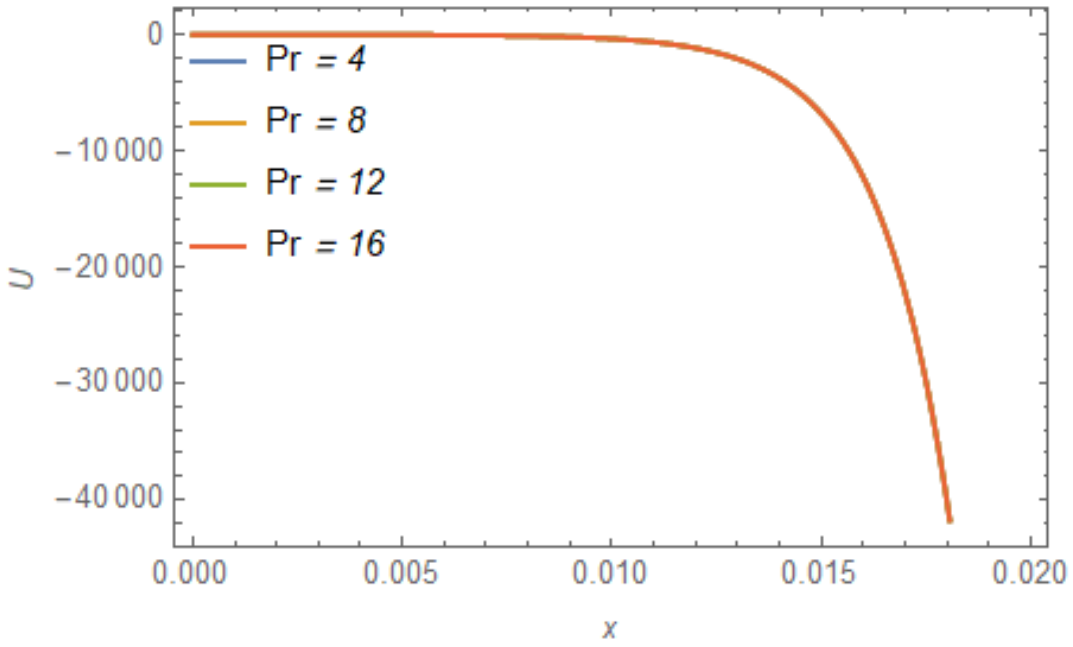

Figure 13. Velocity profile against axial distance for increasing Prandtl number.

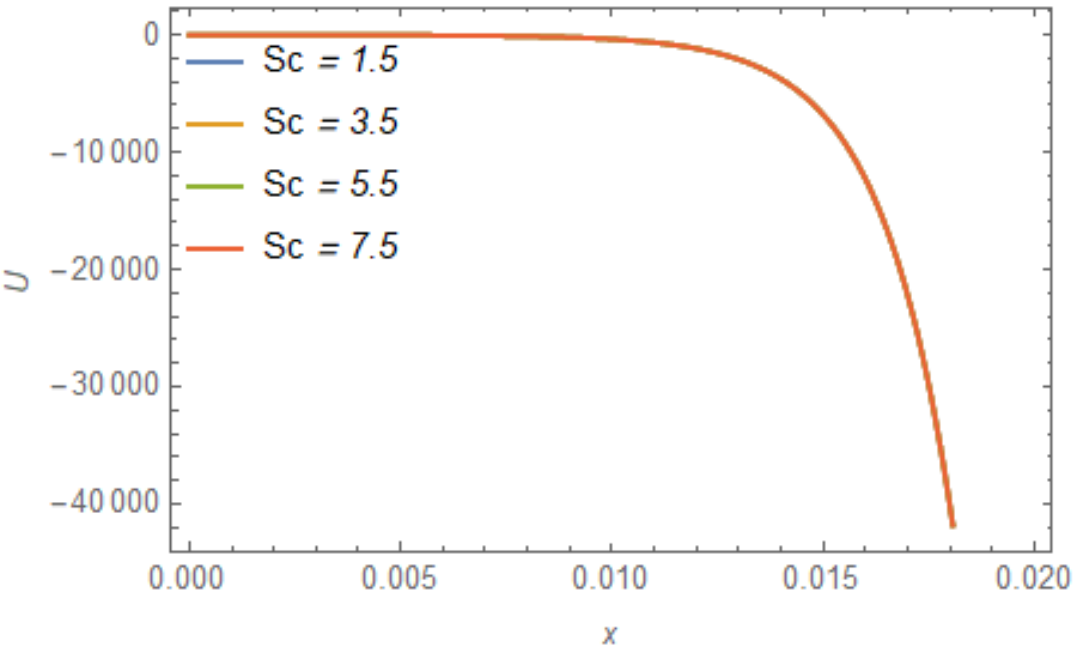

Iron (II, III) oxide nanofluid decreases along the axis for all values of the Prandtl number. Results presented by Kataria and Mittal (2015) and Kataria and Mittal (2017) state that there is a drop in velocity as the Prandtl number increases.

In Figure 14, the physical situation is shown when the velocity profile is plotted along the axis for increasing Schmidt number values. The profile's result trend shows how the water-based Iron (II, III) oxide's velocity drops as Schmidt number values rise progressively. The pattern of results further demonstrates that, for all Schmidt number values, the velocity of the Iron (II, III) oxide nanofluid drops along the axis. The result agrees with the report presented by Kataria and Mittal (2017).

In Figure 15, the graphical profile of velocity along the axis is shown for increasing values of the Reynolds

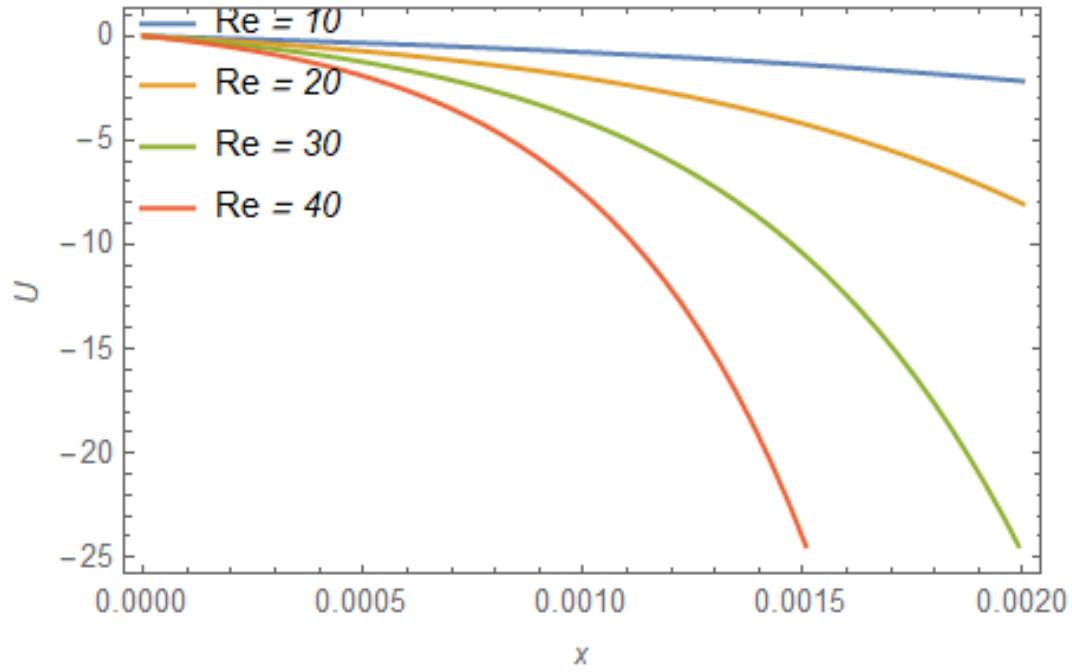

Figure 15. Velocity profile against axial distance for increasing Reynolds number.

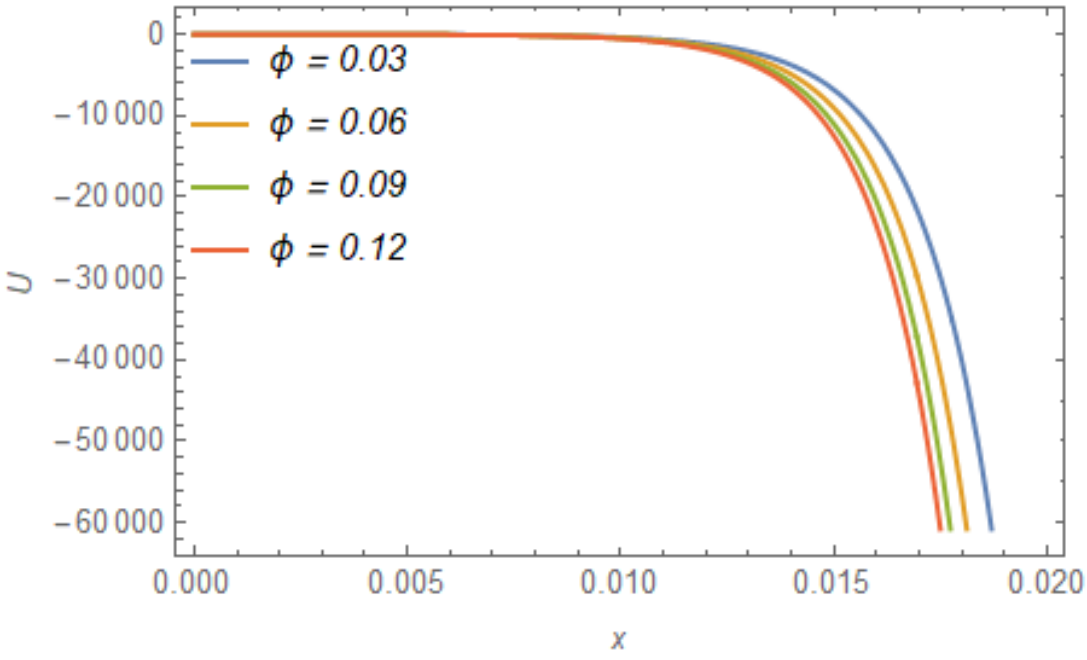

Figure 16. Velocity profile against axial distance for increasing nanoparticle volume fraction.

number. The behaviour of the results in the profile reveals how the velocity of the water-based iron (II, III) oxide decreases with a successive increase in the values of the Reynolds number. The pattern of results presented also shows that the velocity of Iron (II, III) oxide nanofluid decreases along the axis for all values of the Reynolds number.

In Figure 16, the pattern of trendlines shows the situation when Iron (II, III) oxide nanofluid is used. The velocity profile is produced graphically for different nanoparticle

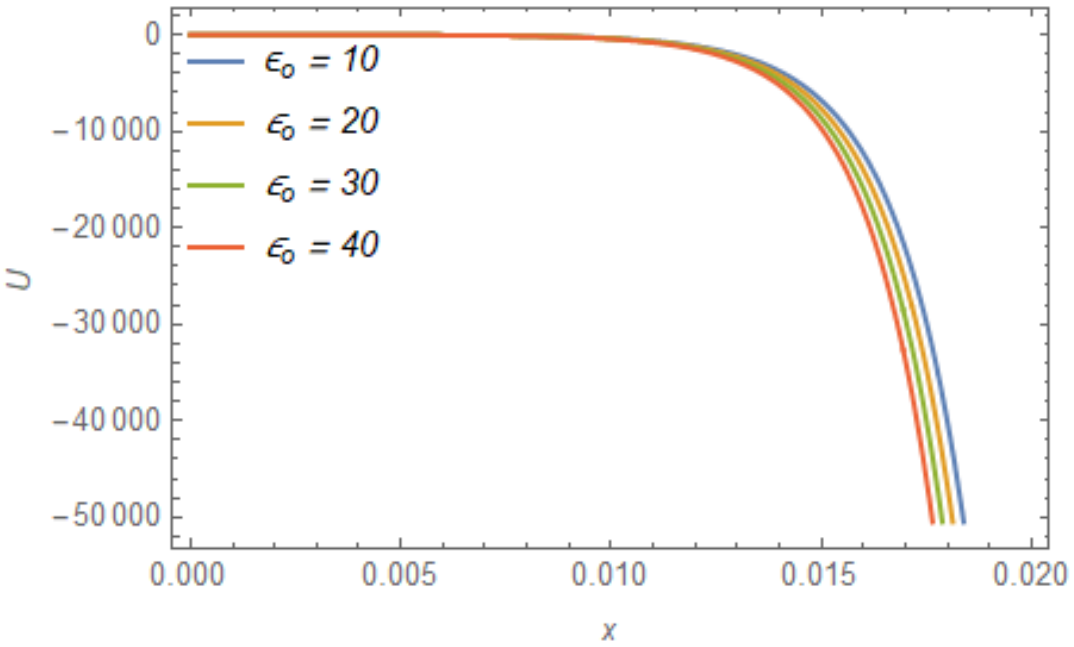

Figure 17. Velocity profile against axial distance for increasing electroconductivity term.

volume fraction values. The profile's pattern of results demonstrates how the water-based Iron (II, III) oxide's velocity increases as the volume of nanoparticles increases. For all values of the nanoparticle volume fraction, the pattern of results also demonstrates that the velocity of the Iron (II, III) oxide nanofluid increases down the axis. The result agrees with the report of Akbarinia (2008), Hosseinzadeh *et al.* (2018), but contrary to the results presented by Mostafazadeh *et al.* (2019), Hady *et al.* (2012), Kataria and Mittal (2017), and Singh *et al.* (2016).

In Figure 17, the results of the velocity field for varying electroconductivity term show trendlines patterns that demonstrate how the velocity field decreases along the axis and diminishes further as the values of the electroconductivity term increase.

Conclusion

According to the mathematical assumption and formalism for nanofluid flow in a rectangular cavity, and using the combined models of thermal conductivity and viscosity, as well as the radiative heat flux vector for an optically thin medium, these conclusions are reached in this study:

1. Increase in nanoparticle volume fraction triggers an increase in concentration. Also, the water-based Iron (II, III) oxide's velocity increases as nanoparticles volume increases.
2. Temperature decreases as the radiation term increases, and the velocity field is unresponsive to the successive increase in values of the radiation term.
3. The mass concentration decreases as the chemical reaction term increases. And the velocity field of the water-based Iron (II, III) oxide overlaps for increasing values of the chemical reaction term.
4. The result pattern from the profile reveals how the velocity of the water-based Iron (II, III) oxide decreases for successive increases in values of thermal Grashof number.
5. The result pattern obtained in the profile reveals how the velocity of the water-based Iron (II, III) oxide decreases for a sequential increase in values of modified Grashof number.
6. The pattern of results in the profile shows how the velocity of the water-based Iron (II, III) oxide increases for successive increases in values of Hartmann number.
7. The velocity fields overlap for a continuous increase in values of the Prandtl number, and decrease along the axis for all values of the Prandtl number. Consequently, there is a decrease in temperature as a result of an increase in the Prandtl number.
8. The velocity field of the water-based Iron (II, III) oxide drops as the Schmidt number value is enhanced. And also drops along the axis. The mass concentration also decreases as displacement along the x-axis alongside the Schmidt number increases.
9. The velocity of the water-based Iron (II, III) oxide along the axis decreases for successive increases in the Reynolds number value.
10. The velocity field decreases along the axis and diminishes further as the values of the electroconductivity term increase.

CONFLICT OF INTEREST

The author states that there is no conflict of interest.

REFERENCES

Abareshi, M., Sajjadi, S. H., Zebarjad, S. M., & Goharshadi, E. K. (2011). Fabrication, characterization, and measurement of viscosity of α-Fe_2O_3-glycerol nanofluids, *Journal of Molecular Liquids*, *163*(1), 27-32.

Akbarinia, A. (2008). Impacts of nanofluid flow on skin friction factor and Nusselt number in curved tubes with constant mass flow, *International Journal of Heat and Fluid Flow*, 29(1), 229-241.

Aminuddin, N. A., Nasir, N. A. A. M., Jamshed, W., Ishak, A., Pop, I., & Eid, M. R. (2023). Impact of thermal radiation on MHD GO-Fe_2O_4/EG flow and heat transfer over a moving surface, *Symmetry*, 15(3), 584.

Batool, S., Rasool, G., Alshammari, N., Khan, I., Kaneez, H., & Hamadneh, N. (2022). Numerical analysis of heat and mass transfer in micropolar nanofluids flow through lid driven cavity: Finite volume approach, *Case Studies in Thermal Engineering*, *37*, 102233.

Bhandari, A. (2023). Analysis of water conveying iron (III) oxide nanoparticles subject to a stationary magnetic field and alternating magnetic field, *Journal of Dispersion Science and Technology*, 44(1), 204-213.

Bhattacharya, P. S. S. K., Saha, S. K., Yadav, A., Phelan, P. E., & Prasher, R. S. (2004). Brownian dynamics simulation to determine the effective thermal conductivity of nanofluids, *Journal of Applied Physics*, *95*(11), 6492–6494.

Boričić, Z., Nikodijević, D., Milenković, D., & Stamenković, Ž. (2005). A form of MHD universal equations of unsteady incompressible fluid flow with variable electroconductivity on heated moving plate. *Theoretical and Applied Mechanics*, *32*(1), 65-77.

Cogley, A. C., Vincenti, W. G., & Gilles, S. E. (1968). Differential approximation for radiative heat transfer in a non-gray gas near equilibrium, *AIAA Journal*, 6(3), 551-553.

Das, S. K., Choi, S. U. S., Yu, W., & Pradeep, T. (2007). *Nanofluids: Science and Technology*. Hoboken, NJ: John Wiley & Sons.

De Bruijn, H. (1942). The viscosity of suspensions of spherical particles. (The fundamental η-c and φ relations). *Recueil des Travaux Chimiques des Pays-Bas*, *61*(12), 863-874.

Dogonchi, A.S., Alizadeh, M., & Ganji, D. D. (2017). Investigation of MHD Go-water nanofluid flow and heat transfer in a porous channel in the presence of thermal radiation effect, *Advanced Powder Technology*, *28*(7), 1815-1825.

Ebaid, M. S., Ghrair, A. M., & Al-busoul, M. (2022). Investigation of heat transfer enhancement using ferro-nanofluids (Fe_3O_4/water) in a heated pipe under the application of magnetic field, *Advances in Mechanical Engineering*, 14(6).

Farooq, U., Hassan, A., Fatima, N., Imran, M., Alqurashi, M. S., Noreen, S., & Bariq, A. (2023). A computational fluid dynamics analysis on Fe_3O_4–H_2O based nanofluid axisymmetric flow over a rotating disk with heat transfer enhancement, *Scientific Reports*, *13*(1), 4679.

Farooq, U., Imran, M., Waqas, H., Alhushaybari, A., Alharthi, A. M., & Noreen, S. (2024). Computational Modeling of Thermal Radiation in Bioconvectional Flow Through Burger Nanofluid with Cattaneo-Christov Heat and Mass Flux Along an Inclined Surface. *Journal of Nanofluids*, *13*(1), 189-198.

Gupta, R., Albidah, A. B., Noor, N. F. M., & Khan, I. (2025). Application of DTM to heat source/sink in squeezing flow of iron oxide polymer nanofluid between electromagnetic surfaces, *Case Studies in Thermal Engineering*, *66*, 105735.

Hady, F. M., Ibrahim, F. S., Abdel-Gaied, S. M., & Eid, M. R. (2012). Radiation effect on viscous flow of a nanofluid and heat transfer over a nonlinearly stretching sheet. *Nanoscale Research Letters*, 7, 1-13.

Hamid, M., Usman, M., Zubair, T., Haq, R. U., & Wang, W. (2018). Shape effects of MoS_2 nanoparticles on rotating flow of nanofluid along a stretching surface with variable thermal conductivity: A Galerkin approach, *International Journal of Heat and Mass Transfer*, *124*, 706-714.

Hassan, M. (2018). Impact of iron oxide particles concentration under a highly oscillating magnetic field on ferrofluid flow. *The European Physical Journal Plus*, *133*(6), 230

Hayat, T., Ullah, H., Ahmad, B. and Alhodaly, M.S. (2021) Heat transfer analysis in convective flow of Jeffrey nanofluid by vertical stretchable cylinder, *International Communications in Heat and Mass Transfer*, 120, p. 104965.

Hosseinzadeh, K., Afsharpanah, F., Zamani, S., Gholinia, M., & Ganji, D. D. (2018). A numerical investigation on ethylene glycol-titanium dioxide nanofluid convective flow over a stretching sheet in presence of heat generation/ absorption. *Case Studies in Thermal Engineering*, *12*, 228-236.

Hsiao, K. L. (2017). Micropolar nanofluid flow with MHD and viscous dissipation effects towards a stretching sheet with multimedia feature, *International Journal of Heat and Mass Transfer*, *112*, 983-990.

Jalili, B., Alamdari, S. G., Jalili, P., & Gani, D. D. (2023) Analysis of bio-nanofluid flow over a stretching sheet with slip boundaries, *Results in Physics*, *54*, 107083.

Khalid, A., Khan, I., & Shafie, S. (2015). Exact solutions for free convection flow of nanofluids with ramped wall temperature. *The European Physical Journal Plus, 130*(4), 57.

Kaneez, H., Baqar, A., Andleeb, I., Hafeez, M. B., Krawczuk, M., Jamshed, W., & Abd-Elmonem, A. (2023) Thermal analysis of magnetohydrodynamics (MHD) Casson fluid with suspended iron (II, III) oxide-aluminum oxide-titanium dioxide ternary-hybrid nanostructures, *Journal of Magnetism and Magnetic Materials*, *586*, 171223.

Kataria, H. R., & Mittal, A. S. (2015) Mathematical model for velocity and temperature of gravity-driven convective optically thick nanofluid flow past an oscillating vertical plate in presence of magnetic field and radiation, *Journal of the Nigerian Mathematical Society*, 34(3), 303-317.

Kataria, H. R., & Mittal, A. S. (2017) Velocity, mass and temperature analysis of gravity-driven convection nanofluid flow past an oscillating vertical plate in the presence of magnetic field in a porous medium, *Applied Thermal Engineering*, *110*, 864-874.

Khalid, A., Khan, I., & Shafie, S. (2015). Exact solutions for free convection flow of nanofluids with ramped wall temperature. *The European Physical Journal Plus*, 130,1-14.

Khan, M. I., Kadry, S., Chu, Y., & Waqas, M. (2021). Modeling and numerical analysis of nanoliquid (titanium oxide, graphene oxide) flow viscous fluid with second order velocity slip and entropy generation, *Chinese Journal of Chemical Engineering*, *31*, 17-25.

Khan, M. S., Mei, S., Shabnam, Fernandez-Gamiz, U., Noeiaghdam, S., Shah, S. A., & Khan, A. (2022). Numerical analysis of unsteady hybrid nanofluid flow comprising CNTs-ferrousoxide/water with variable magnetic field, *Nanomaterials*, *12*(2), 180.

Koriko, O. K., Adegbie, K. S., Animasaun, I. L., & Ijirimoye, A. F. (2020) Comparative analysis between three-dimensional flow of water conveying alumina nanoparticles and water conveying alumina–iron (III) oxide nanoparticles in the presence of Lorentz force, *Arabian Journal for Science and Engineering*, 45, 455-464.

Krishna, M. V., Ahammad, N. A., & Chamkha, A. J. (2021). Radiative MHD flow of Casson hybrid nanofluid over an infinite exponentially accelerated vertical porous surface. *Case Studies in Thermal Engineering*, *27*, 101229.

Kumar, D. H., Patel, H. E., Kumar, V. R., Sundararajan, T., Pradeep, T., & Das, S.K. (2004) Model for heat conduction in nanofluids, *Physical Review Letters*, *93*(14), 144301.

Madhukesh, J. K., Ramesh, G. K., Chavaraddi, K. B., Aly, E. H., Almutairi, B., & Shah, N. A. (2023) Impact of active and passive control of nanoparticles in ternary nanofluids across a rotating sphere, *Results in Physics*, *54*, 107069.

Mahian, O., Kianifar, A., Kalogirou, S. A., Pop, I., & Wongwises, S. (2013) A review of the applications of nanofluids in solar energy, *International Journal of Heat and Mass Transfer*, *57*(2), 582-594.

Mostafazadeh, A., Toghraie, D., Mashayekhi, R., & Akbari, O. A. (2019) Effect of radiation on laminar natural convection of nanofluid in a vertical channel with single- and two-phase approaches. *Journal of Thermal Analysis and Calorimetry*, *138*(1), 779-794.

Muritala, A. O., Adio, S. A., Luqman, O., Adebayo, O. S., Akinlolu, I. J., & Obayopo, S.O. (2022) Experimental study on effect of magnetic field on flow dynamics of iron (III) oxide (Fe_2O_3) water based nanofluid using Taylor Couette flow apparatus. *Nigerian Journal of Technology*, *41*(3), 454-463.

Ngiangia, A. T., & Jim-George, F. L. (2019). Effect of electro-thermal conductivity on MHD free convection flow in an inclined porous channel. *Journal of Information and Optimization Sciences*, *40*(6), 1265-1279.

Ngiangia, A. T., & Nwabuzor, P. O. (2019). Electro conductivity of generalized MHD Burgers fluid flow due to a sinusoidal accelerating plate. *Science & Technology*, *5*, 195-204.

Ngiangia, A. T., & Okechukwu, A. (2016) Influence of variable electroconductivity and radiation on MHD Couette flow. *World Scientific News*, *2*(47), 241-253.

Nield, D. A., & Bejan, A. (2006) *Convection in Porous Media*. 3rd edition. New York: Springer.

Ojjela, O. (2022) Numerical investigation of heat transport in Alumina–Silica hybrid nanofluid flow with modeling and simulation. *Mathematics and Computers in Simulation*, *193*, 100-122.

Rammoorthi, R., & Mohanavel, D. (2023) Influence of radiative magnetic field on a convective flow of a chemically reactive hybrid nanofluid over a vertical plate. *Journal of Advanced Research in Fluid Mechanics and Thermal Sciences*, *105*(1), 90-106.

Rout, B. C., & Mishra, S. R., (2019). An analytical approach to the metal and metallic oxide properties of Cu–water and TiO 2–water nanofluids over a moving vertical plate. *Pramana*, 93(3), 41.

Sadeghi, S. S., Hadi, A., & Mashhadi, M. M. (2023). Viscosity of Fe_2O_3-water nanofluids by molecular dynamics simulations: Effects of nanoparticle content, temperature and size. *Journal of Molecular Liquids*, *382*, 121859.

Shima, P. D., Philip, J., & Raj, B. (2010) Synthesis of aqueous and nonaqueous iron oxide nanofluids and study of temperature dependence on thermal conductivity and viscosity. *The Journal of Physical Chemistry C*, *114*(44), 18825-18833.

Singh, K., Rawat, S. K., & Kumar, M. (2016) Heat and mass transfer on squeezing unsteady MHD nanofluid flow between parallel plates with slip velocity effect. *Journal of Nanoscience*, Volume 2016, Article ID 9708562, 11 pages.

Tiwari, R. K., & Das, M. K. (2007) Heat transfer augmentation in a two-sided lid-driven differentially heated square cavity utilizing nanofluids. *International Journal of Heat and Mass Transfer*, *50*(9-10), 2002-2018.

Vand, V. (1948) Viscosity of solutions and suspensions. I. Theory. *Journal of Physical and Colloid Chemistry*, *52*(2), 277-299.

Yahya, N., Kashif, M., Shafie, A., Soleimani, H., Zaid, H. M., & Latiff, N. R. A. (2014). Improved oil recovery by high magnetic flux density subjected to iron oxide nanofluids. *Journal of Nano Research*, 26, 89-99.